In Vitro Growth of Bioactive Nanostructured Apatites via Agar-Gelatin Hybrid Hydrogel

Yi Deng[1,2], Xianghui Zhao[1], Yongsheng Zhou[1], Peizhi Zhu[2,4], Li Zhang[3,*], and Shicheng Wei[1,2,*]

[1] *Department of Prosthodontics, Laboratory of Interdisciplinary Studies, School and Hospital of Stomatology, Peking University, Beijing 100081, People's Republic of China*
[2] *Center for Biomedical Materials and Tissue Engineering, Academy for Advanced Interdisciplinary Studies, Peking University, Beijing 100871, People's Republic of China*
[3] *Analytical and Testing Center, Research Center for Nano-biomaterials, Sichuan University, Chengdu 610064, People's Republic of China*
[4] *Department of Chemistry, University of Michigan, Ann Arbor, Michigan 48109-1055, United States*

Biomimetic synthesis of bone-like carbonated apatite with good biocompatibility is a promising strategy for the development of novel biomaterials for bone engineering applications. Most research efforts have been focused on only protein-based or only polysaccharide-based template for synthesis of apatite minerals. To understand the cooperative roles of gelatin and polysaccharide playing in the biomineralization, agar hydrogel, gelatin and agar-gelatin hybrid hydrogel were respectively introduced as mineralization matrix for the *in vitro* growth of apatite in the study. It was shown that bundle-like carbonated apatite was successfully prepared in agar-gelatin hybrid hydrogel for the first time, through the interaction between apatite and matrix macromolecule under physiological temperature. Moreover, the *in vitro* biocompatibility of the prepared nanostructured apatite crystals was investigated using CCK-8 assay and alkaline phosphatase activity of osteoblast-like MC3T3-E1. Compared with HA synthesized by traditional method, the obtained apatite in agar-gelatin hybrid hydrogel could provide significantly higher cell viability and alkaline phosphatase activity. Through the study, we could better understand the role of gelatin and polysaccharide in bone formation process, and the product is a promising candidate to be used in bone tissue engineering.

KEYWORDS: *Carbonated Apatite, Agar-Gelatin Hydrogel, Self-Assembly, Biocompatibility, Bone Tissue Engineering.*

INTRODUCTION

Hard tissues of human body such as bone have a complex structure, and are composed of approximately 70% minerals and 30% organic matrix by dry weight.[1,2] The mineral crystals in human bone tissue grow with a specific crystalline orientation-extremely elongated in the *c*-axial direction, high aspect ratio and packed in parallel arrays. At the finer end of the hierarchical spectrum of bone, the self-assembled collagen fibrils are impregnated with bundle structures of apatite nanocrystals having tens of nanometers in length and width.[3]

Recently, various kinds of nanostructured materials, such as synthesis nano-polymeric scaffolds,[4,5]

nanovesicles,[6] carbon nanotube[7,8] and silica,[9] have been applied in bone tissue engineering, however, they are not the intrinsic constituents of our body, which makes potential implantation applications problematic. Hydroxyapatite (HA) is the basic component of the natural bone, and is widely considered to be the ideal bone graft substitutes in bone tissue engineering,[10,11] due to its excellent osteoinduction[12] and chemical similarity with bone apatite. So far, various methods have been reported to produce nanostructured HA crystals, including chemical precipitation process,[13,14] solid-state reaction,[15] and sol–gel synthesis.[16] However, these approaches can't control the crystal morphology precisely, and the structure and morphology of the obtained nanostructured HA crystals often differ from those of bone apatite. Besides, HA crystals prepared by the conventional approach have low biocompatibility and induce apoptosis in osteoblasts with the concentration beyond 20 μg/mL.[17] To reduce the

inflammation of HA coating, it was reported that platelet-rich plasma and platelet-rich fibrin were pre-grafted into the bone defects before putting the HA coated implants.[18] Therefore, currently researchers are concentrating on synthesizing nanostructured carbonated apatite with specific structure and good bioactive property similar to those of bone apatite.

The organics in bone contain both proteins and polysaccharides, in which the former being the focus of most studies to explore the theory of bone mineralization.[19] Most researches on bone biomimetic mineralization were focused on collagen,[20, 21] gelatin[22, 23] and peptides.[24] Wang[21] demonstrated that collagen played an active role in the oriented HA formation in bone. Recently, it was reported that organic matrix such as polysaccharide played a key role in providing a favorable environment for the growth of oriented apatite.[19] A rational biomimetic design demonstrated that an acidic polysaccharide was very important in regulating the morphology, size and crystallinity of minerals, through the functional groups of polysaccharide chelating Ca^{2+}.[25] However, only protein (e.g., collagen and gelatin) or polysaccharide can hardly compare to the complex surrounding of biomineralization. Meanwhile, the modulation role of gelatin and polysaccharide on composition and morphology of calcium phosphate crystals is still unclear, especially the mechanism of how to co-control the oriented nano-assembled structure of apatite crystals.

Hererin, in the study, we will first focus on the apatite crystallization using agar-gelatin hybrid hydrogel to understand the cooperative effects of gelatin and polysaccharide on the formation of apatite. The hydrogel network is an excellent system to study the crystallization because (a) gelatin could be incorporated into the hydrogel and remain stable during the experiment, (b) the local concentration for crystallization is readily achievable and (c) the deposits are easily harvested from the medium without agar contamination.[26–28] In our work, apatite crystals modulated in the presence of agar-gelatin hybrid hydrogel will be prepared, and the effects of obtained apatite on the viability and osteogenic differentiation of MC3T3-E1 cells will also be assessed through CCK-8 and alkaline phosphate activity assay.

MATERIALS AND METHODS
Materials

$Ca(NO_3)_2 \cdot 4H_2O$ (AR), $Na_2HPO_4 \cdot 12H_2O$ (AR), NaOH (AR) and CH_2CH_3OH (AR) were provided by Sinopharm Chemical Reagent Co., Ltd. (Beijing, China). Agar powder $((C_{12}H_{18}O_9)_n)$ was purchased from Biodee Biotechnology Co., Ltd. (Tokyo, Japan), and Gelatin (from porcine skin, G1890-100G) was purchased from Sigma-aldrich (St. Louis, USA). All other chemicals were of analytical grade and used as received. All aqueous solutions were prepared with de-ionized water (D.I. water).

Preparation of Hydrogels

Pure agar hydrogel was synthesized according to the following method: 2% (w/v) of agar was dissolved in $Ca(NO_3)_2$ solution at 100 °C with continuous stirring. The boiled solution was immediately defoamed ultrasonically, and pH value was adjusted to 10 by adding NaOH solution. Then the mixture was kept stirring vigorously for 2 h. Afterwards the homogeneous solution was immediately transferred into a refrigerator at 5 °C for 3 h to get an agar hydrogel.

Agar-gelatin hybrid hydrogel was fabricated as follows: firstly, the boiled agar solution containing $Ca(NO_3)_2$ was prepared according to the above-mentioned method and cooled to 50 °C. Then 1% (w/v) gelatin was added into the mixture at 50 °C with continuous stirring, and the pH was also adjusted to 10. After that, the mixture was kept stirring vigorously for 2 h to allow Ca^{2+} ions to thoroughly bind with the carboxyl groups on gelatin. Finally, the agar-gelatin hybrid hydrogel was formed by rapid cooling to 5 °C.

Synthesis of Carbonated Apatite in Hydrogels

Apatite crystals were synthesized in agar hydrogel with or without gelatin under physiological or higher temperature environment. Phosphate solution was added on the top of the hydrogel containing calcium ions according to the resulting Ca/P ratio of 1.67. Crystal growth in hydrogel occurred when kept at 37 °C and 65 °C, and the pH value was maintained at 10 throughout the process. This hydrogel system, known as a single diffusion system, continuously operated for 3 days, and a layer of white periodically arranged growth areas (called Liesegang bands)[29] was seen at the interface of PO_3^{4-} solution and Ca^{2+} hydrogel. After mineralization, the supernatant solution was removed, and the mineralized hydrogels were immersed in D.I. water for 48 h to remove residual ions. Prior to SEM observation, the samples were carefully removed from the interface and washed with D.I. water 3 times without shaking. For other characterizations, the isolated samples containing Liesegang segments were heated to 50 °C with D.I. water. Further, the products were cleaned by washing with warm water and ethanol, respectively, and then centrifuged several times until the impurities were completely removed. Then the obtained products were dried at 60 °C.

Direct synthesis of apatite in gelatin solution and by wet chemical method in the absence of agar and gelatin were also compared as control groups. The specific synthetic conditions for each sample are listed in Table I.

Measurements

The crystalline phase of prepared powders were identified and analyzed by X-ray diffraction (XRD, Shimadzu, Japan) using a Cu target as radiation source ($\lambda = 1.540598$ Å) at 40 kV. The diffraction angles (2θ) were set between 20° and 60°, incremented with a step size of 4 °/min.

Table I. Synthesizing conditions for preparing the carbonated apatite in all cases.

Sample name	Agar (w/v%)	Gelatin (w/v%)	Time hours	Temperature (°C)	Synthetic method
Agar37	2	0	72	37	Mineralization
Agar65	2	0	72	65	Mineralization
Agar-gelatin37	2	1	72	37	Mineralization
Agar-gelatinl65	2	1	72	65	Mineralization
Gelatin37	0	1	72	37	Agitation
Gelatin65	0	1	72	65	Agitation
Pure HA	0	0	72	65	Agitation

Unmineralized and mineralized hydrogels were freeze-dried in a lyophilizer at $-40\ ^\circ C$ for 48 h. Then the feeze-dried hydrogels were ground into powder, mixed with KBr, and compressed into KBr pellets. Fourier transform infrared spectra (FTIR) were then obtained with Nicolet Magna IR 750 spectrometer recorded from 4000 to $400\ cm^{-1}$.

X-ray photoelectron spectroscopy (XPS, AXIS Ultra, Kratos Analytical Ltd.) was employed to identify the chemical constituent and elemental state of the prepared apatite. The binding energies were calibrated by the C1s hydrocarbon peak at about 285 eV. The quantitative analysis and the curve fitting were conducted by the CasaXPS software package.

Thermogravimetric analysis (TG, Q600-SDT, USA) was carried out to determine the actual yield of organic matrix on the surface of apatite, and approximately 5 mg of the powder was heated from $25\ ^\circ C$ to $1000\ ^\circ C$ with a heating rate of $10\ ^\circ C/min$. All samples were carried out under a nitrogen atmosphere with an empty Al_2O_3 crucible as a reference.

The freeze-dried hydrogel specimen before and after mineralization were cut using a razor and coated with gold for surface morphology observation with a field-emission scanning electron microscope (ESEM, AMRAY 1-1910FE). However, for the obtained apatite from gelatin solution and wet chemical method, the suspension of the powder was deposited on Si wafers. The SEM facility was also equipped with an EDX energy-dispersive spectrometer for microchemical analysis.

Microstructural morphology was also carried out using Tecnai F20 transmission electron microscope (TEM) with an accelerating voltage of 200 kV. Samples for TEM imaging were prepared by dropping the powder suspension (the suspension was diluted in ethanol, and dispersed ultrasonically) onto carbon-coated copper grid. Selected area electron diffraction (SAED) was also recorded.

Cell Culture

Mouse pre-osteoblast cells (MC3T3-E1, American Type Culture Collection, USA) were cultured in α-Modified Eagle's Medium (αMEM, Gibco, CA) containing 10% fetal bovine serum (FBS, Gibco), 100 μg/mL streptomycin (Amresco, Cleveland, USA) and 100 μg/mL penicillin (Amresco) at $37\ ^\circ C$ in a humidified atmosphere of 5% (v/v) CO_2 incubator (MCO-18AIC, Japan).

Cell Viability Assay

Viability of MC3T3-E1 cells was assessed using the cell counting kit-8 assay (CCK-8, Dojindo). After cell counting, MC3T3-E1 cells were seeded in 96-well culture plates (Costar, USA) at a density of 5×10^3 cells/well. After seeding 24 h, cells were exposed to the 200 μL medium containing different apatite with the concentration of 20 μg/mL or 200 μL pure medium (control) or 200 μL medium containing 10% dimethyl sulfoxide (positive group). After incubating for 1, 3, 5 days, 10 μL of CCK-8 was added into each well for 4-hour incubation. Then 80 μL of supernatant from each well was transferred to new 96-well cell culture dishes. The absorbance value (OD value) was measured at 450 nm with a microplate reader (Model 680, Bio-Rad, Hercules, CA).

Alkaline Phosphate Activity Assay

Alkaline phosphatase (ALP) activity of MC3T3-E1 cells was evaluated by an assay reagent kit (Nanjing Jiancheng Bioengineering Institute, China). At the end of the incubation, cells were exposed to different apatite media with the concentration of 20 μg/mL for 7 days. Cellular alkaline phosphatase activity was determined in terms of the initial rates of hydrolysis of *p*-nitrophenyl phosphate (Amresco) to *p*-nitrophenol. Briefly, the supernatant was removed and 100 μL of lysis solution (1% TritonX-100) was added into each well and incubated for 1 h. Afterwards, 30 μL of MC3T3-E1 cell lysates at each well was transferred to new 96-well cell culture dishes, and cultivated with 50 μL of carbonated buffer solution (pH = 10) and 50 μL of substrate solution (4-amino-antipyrine) at $37\ ^\circ C$ for 15 min. Then 150 μL of potassium ferricyanide (chromogenic agent) was added into the above solution and the production of *p*-nitrophenol was determined by the absorbance at 405 nm in a microplate reader. For normalization, the total protein concentration was measured by a Bicinchoninic Acid (BCA) protein assay kit (Beijing Biosea Biotechnology, China). Thus, alkaline phosphatase activity was normalized and expressed as the total protein content (U/gprot).

Statistical Analysis

All data were expressed as mean $\pm$ standard deviations derived from experiments carried out in triplicate. Statistical analysis was performed with Origin software. Student's

t-test was used to determine the significant differences among the groups, and *p*-values less than 0.05 were considered statistically significant.

RESULTS AND DISCUSSION

Figure 1 illustrates the mineralization of agar-based hydrogel scaffolds. Calcification started immediately on the interface between hydrogel and solution as soon as the phosphate solution was loaded on the hydrogel. As shown in Figure 1(a), due to Ca^{2+} ions binding with the carboxyl groups on agar-gelatin hybrid hydrogel, calcium phosphate crystals precipitated in hydrogel matrix by the single-directional diffusion of PO_4^{3-} ions. At the third day, apatite aggregates formed inside the hydrogel with periodically arranged growth areas (Fig. 1(b)), so-called Liesegang bands.[29] Figure 1(c) shows the porous structure of the agar-gelatin hybrid hydrogel, with pore size ranging from 100 to 300 μm in diameter and a porosity of 92% calculated by the liquid displacement method after being freeze-dried.

Chemical Composition of Carbonated Apatite

X-ray Diffraction Analysis

Figure 2 shows the XRD patterns of all synthesized apatites. The diffraction peaks of the products prepared by agar-gelatin hydrogel and by only gelatin are agreed with those of pure HA at 2θ values of 25.9°, 31.8°, 46.7°, 49.5° and 53.1° corresponding to (002), (211), (222), (213) and (004) planes, respectively, confirming that the obtained products are predominantly HA (JCPDS #09-0432). However, these peaks of apatite in agar hydrogel are widened, indicating that the crystallinity is weak due to the lack of active sites for calcification. It is obvious that the relative
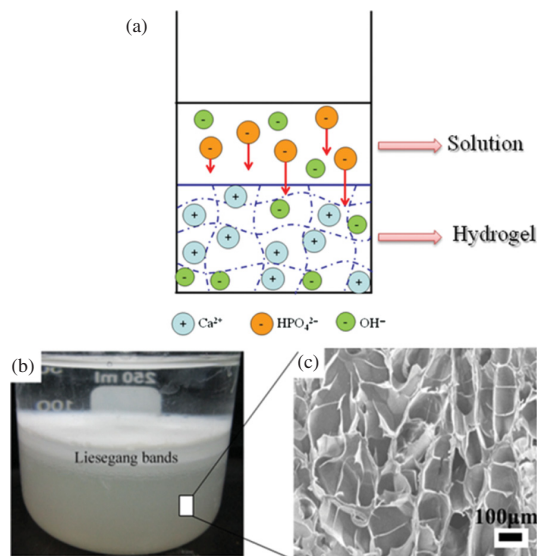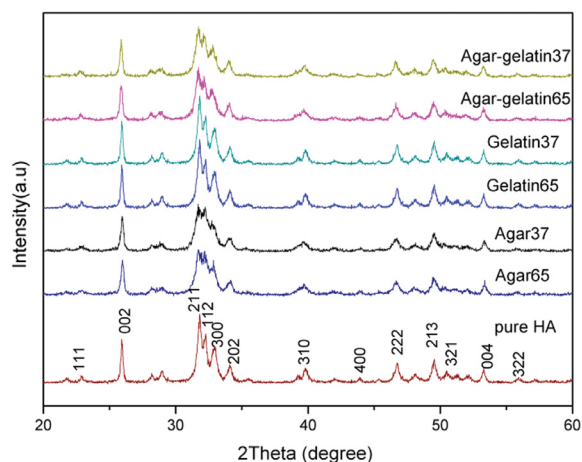

Figure 2. XRD spectra of as-prepared apatite under different conditions.

intensity of diffraction peaks, particularly the peaks corresponding to (211), (112) and (300) planes are increased when gelatin is added into pure agar hydrogel, implying that the crystallinity of apatite is enhanced, and the XRD spectra of the apatite are very similar to that of bone apatite.[10, 30] Nevertheless, the XRD peaks of as-prepared HA in gelatin solution is similar to that of pure HA, implying that gelatin could guide the HA growth with more perfect crystal structure through the interaction between COO^- of gelatin and Ca^{2+} of apatite.[31]

Fourier Transform Infrared Spectroscopy Analysis

The FTIR spectra of all mineralized hydrogels are shown in Figure 3. The absorption peak located at 1041 cm^{-1} originates from the triple ν_3 asymmetrical P–O stretching from apatite, and the peaks at 602 and 562 cm^{-1} could be attributed to the triple ν_4 vibration of PO_4^{3-}.[32] The broad peak at 3441 cm^{-1} is associated with OH^-.[33] The peaks at 1650, 1555 and 1254 cm^{-1} are assigned to the C=O stretching from amide I, N—H deformation from amide II and C—N from amide III, respectively.[34] In addition, the weak peak at 3280 cm^{-1} belongs to the absorption of amide A, and the peak at 2932 cm^{-1} is attributed to the asymmetric vibration of $-CH_2$-.[34] On the other hand, the band of CO_3^{2-} originating from atmosphere is observed at 1384 cm^{-1}, indicating that carbonate has been incorporated into the lattice of apatite and formed B-type carbonate apatite with similarity to the bone apatite.[35, 36]

Additionally, it is noteworthy that FT-IR spectra exhibit a slight shift of C=O band from 1653 cm^{-1} to 1640 cm^{-1} (Fig. 3(b)) when gelatin is added into agar hydrogel, implying that chemical interactions have occurred between Ca^{2+} of apatite and COO^- groups of gelatin. However, the interaction between $-NH_2$ of gelatin and PO_4^{3-} of apatite is hardly detected because it is too weak.[37] It is evident from the above results that the presence of intermolecular

Figure 1. (a) Schematic drawing for the mineralization of hydrogel. (b) The digital photo and (c) SEM micrograph of 3D porous hydrogel scaffold fabricated by freeze drying.
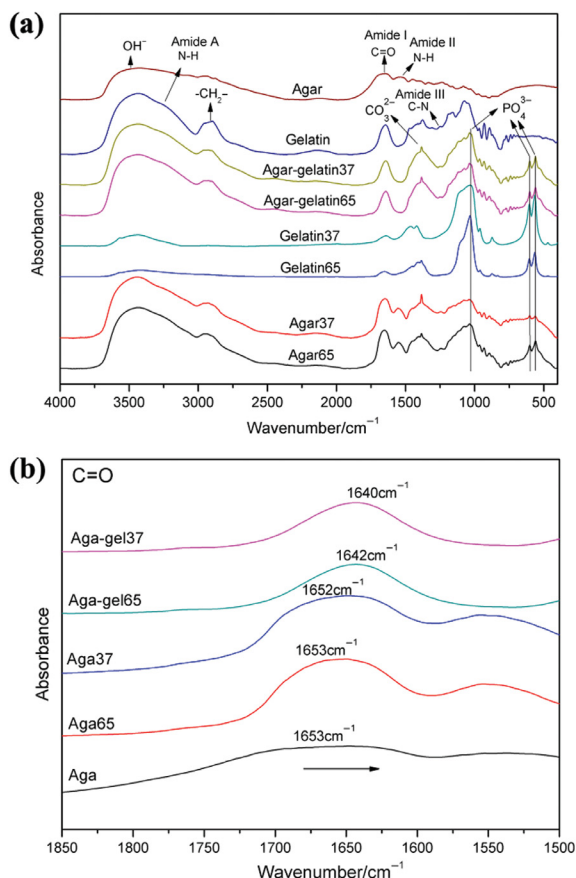
(a)

(b)

Figure 3. (a) FTIR spectra of mineralized hydrogels under different conditions; (b) a shift of C═O band in FT-IR enlarged patterns.

interactions between inorganic/organic phases is helpful to control the nucleation and the orderly growth of inorganic crystals.

X-Ray Photoelectron Spectroscopy

The XPS wide scan in Figure 4(a) shows the peaks of Ca, P, O and small amount of C elements in all samples. The N presence in apatite synthesized in agar-gelatin hydrogel shows that there is some residual gelatin on the surface of apatite crystal. Typically, the high-resolution spectrum of C1s in pure HA and Agar37 groups (Figs. 4(b)–(c)) are deconvoluted into three different curves. The binding energies centered at about 284.8, 286.4 and 289.0 eV are assigned to the carbon skeleton (—C—C—/—C—H—), hydroxyl group (—C—OH) and carbonyl group (—C═O),[38] respectively, whereas the broad peak of —C—N— at about 285 eV is recorded on both Agar-gelatin37 and Gelatin37 samples, indicating the presence of gelatin on the surface of apatite. Additionally, after adding gelatin into agar, the intensity of the carbon skeleton (—C—C—/—C—H—) decreases dramatically, and the peaks of the carbonyl group (—C═O) and

—C—N— bond are increased, as shown in Figure 4(f), which is attributed to the abundant peptide bonding (—NH—C═O) in gelatin, suggesting that the increase of polar functional groups (such as carboxyl, carbonyl and amino) from gelatin could create more reactive sites and defects for the nucleation and growth of nanostructured apatite.[39]

TG Analysis

The TG curves of all obtained apatite are shown in Figure 5. Thermal decomposition residue of organic matrix absorbed on apatite surface can be identified by an exothermal reaction and its corresponding weight loss. It shows that the as-prepared apatite has a multistep thermolysis. The initial weight loss of these samples around 100 °C may be ascribed to the evaporation of absorbed water. Pure HA suffers a very slow weight loss process from room temperature to 1000 °C. On the contrary, there are a sharp weight loss between 200 °C and 650 °C for the apatite synthesized from agar-based hydrogel and gelatin solution, which is attributed to the decomposition of the absorbed organic matrix. Due to the high thermal stability of HA,[40] the incinerated residue of the prepared powder is mainly HA. Therefore, the composition of these samples could be induced through TG analysis, that is, Gelatin37 contains about 7.4 wt% organics, Agar37 contains about 8.3 wt% organics and Agar-gelatin37 contains about 9.7 wt% organics.

Morphology Analysis by SEM and TEM

The unmineralized hydrogels show interconnected pore structures with sizes of 150–500 μm for agar hydrogel and 100–300 μm for agar-gelatin hybrid hydrogel (Figs. 6(a) and (d)). The macropores in agar-based hydrogel could provide a favorable 3D environment to promote the internal mineralization, while the interconnected pores serve for the delivery of ions.[26] After mineralization for 3 days, the interior structure of the hydrogel is not so porous because the pore wall is covered by inorganic deposits. Energy-Dispersive X-ray (EDX) spectroscopy further confirms the presence of Ca and P elements assigning to apatite in the inorganic phase, which is in accordance with FTIR and XRD results. From SEM images, it is clear that the morphologies of apatite formed in different hydrogels are very different, as shown in Figure 6. The flake apatite crystals are appeared in agar hydrogel, while the apatite on agar-gelatin hydrogel has a needle-like morphology. Also, temperature influences the formation and morphology of apatite apparently. We can find that flower-like apatite spherulites have formed on agar hydrogel at physiological temperature (37 °C), and these spheroids are the aggregation of numerous dense and flake-shaped nano-crystals (Fig. 6(b)). Nevertheless, at 65 °C, we could see that the oriented flake-shaped apatite crystals grow perpendicular to the surface of agar hydrogel. Maybe it is because different reaction temperature would provide different Gibbs
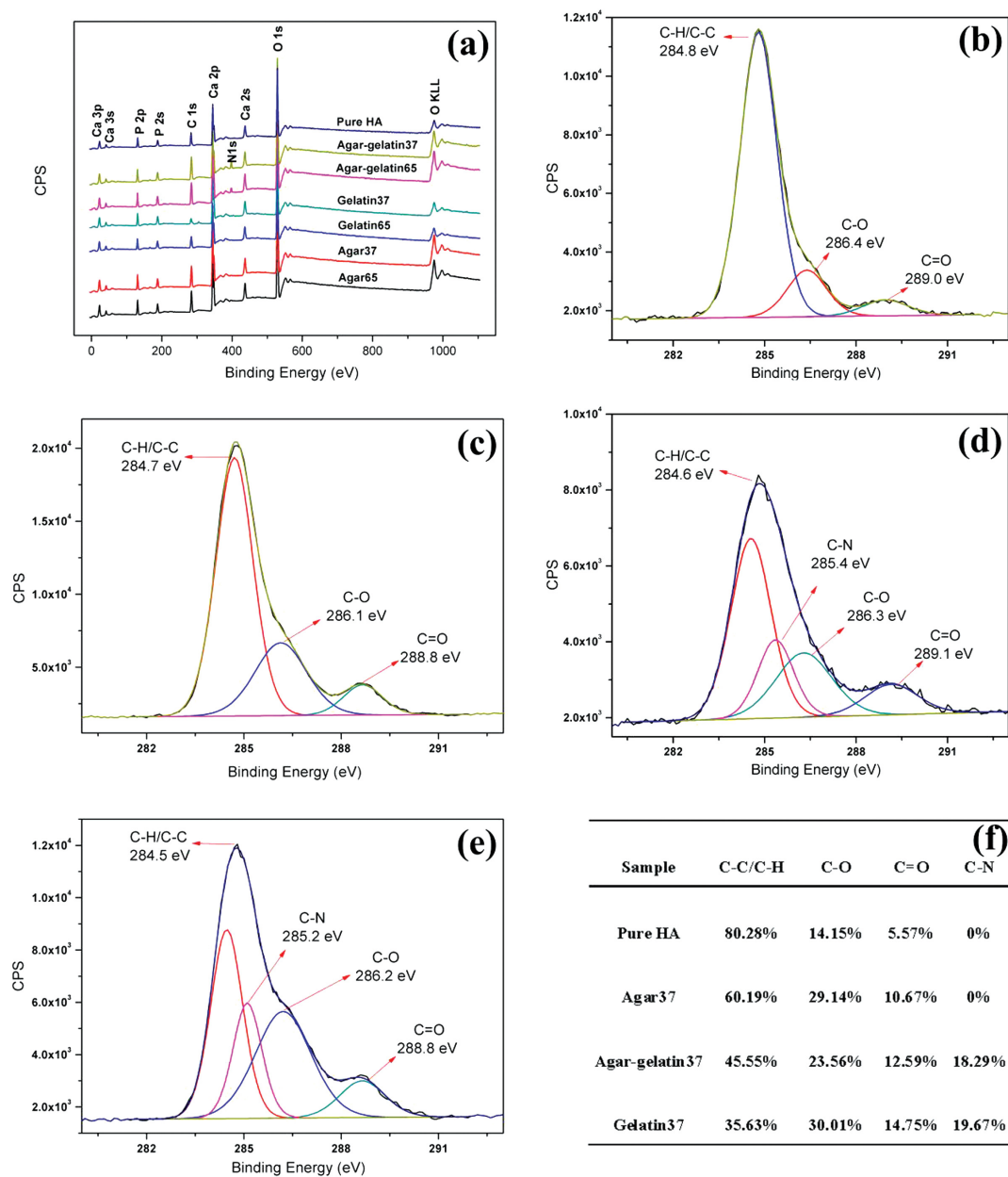
Figure 4. Surface atomic composition of as-prepared apatite under different conditions: XPS wide spectrum of all samples (a); high-resolution spectrum of carbon peaks (C1s) for pure HA (b), Agar37 (c), Agar-gelatin37 (d) and Gelatin37 (e); and the contents of relative functional groups (f).

energy, thus leading to different final hierarchical nanostructure of apatite crystals.[41] In addition, many crystal bundles made up of numerous rod-like crystals could be observed on agar-gelatin hydrogel at 37 °C (Fig. 6(e)). While needle-like apatite crystals for Agar-gelatin65 are uniformly distributed on agar-gelatin hydrogel (Fig. 6(f)). Furthermore, EDX data (Fig. 6(B)) showed that the Ca/P ratio of the inorganic synthesized in agar hydrogel is 1.36, close to octacalcium phosphate (OCP).[42] Whereas Ca/P

ratio of crystals prepared in agar-gelatin hybrid hydrogel is slightly lower than 1.67 of stoichiometric HA, but very close to that of bone apatite, which are thought to be highly bioactive.[43]

As we known, gelatin undergoes a thermal degradation and its single helix chain will break into pieces under a temperature above 60 °C.[44] To understand how the gelatin and its degradation product influence the morphology of apatite crystals, we directly synthesized apatite crystals in
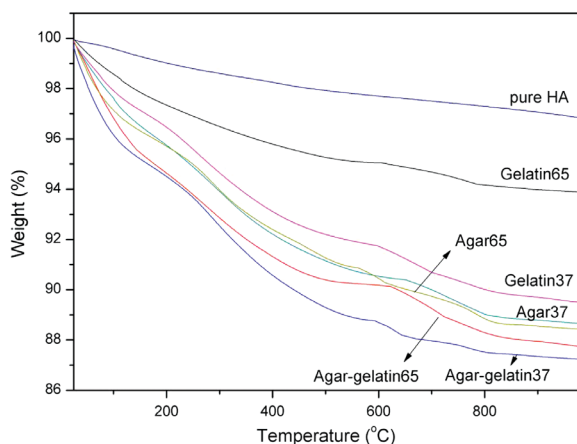
Figure 5. TGA profiles of as-prepared apatite under different conditions.

gelatin solution and their morphology was also investigated. It is found that the obtained HA by wet chemical method shows irregular morphology (Fig. 6(i)), and the apatite crystals prepared in gelatin at 37 °C are uniform rod-like (Fig. 6(g)). But if the temperature is raised to 65 °C, we could see that the apatite crystals demonstrate well-proportioned needle-like morphology with smaller size, as shown in Figure 6(h), suggesting that gelatin degradation could lead to smaller size of apatite crystals.

To verify the results obtained from SEM, TEM equipped with SAED is employed to make clear the microstructure of the apatite. As shown in Figure 7, the morphologies of Agar37 and Agar65 are flake-shaped and have a larger surface area (Figs. 7(a) and (d)), illustrating that the apatite crystals grow in all directions without a nucleation location of Ca^{2+}. Rod-like crystals are shown in Gelatin37, while needle-like apatite crystals with smaller size appear in random orientation in Gelatin65, further testifying the influence of gelatin degradation product on the size of apatite. The morphology of Agar-gelatin37 is distinctly different from other apatite crystals, showing that the bundle structures are made of many small rods aligned parallel to each other (Fig. 7(c)), which is similar to structure of bone apatite.[3,45] This illustrates that carbonated apatite might self-assemble to bone-like apatite modulated by agar-gelatin hybrid hydrogel under physiological temperature. However, Agar-gelatin65 also displays needle-like apatite similar to Gelatin65 (Figs. 7(e) and (f)) due to the degradation of gelatin. Moreover, SAED patterns in Figure 7 insets exhibit strong concentric rings appointed to the (002), (211) and (300) planes of apatite. The lattice fringes of (100) plane with the lattice spacing of about 0.831 nm for bone-like Agar-gelatin65 apatite are shown in HRTEM images (Fig. 7(i)), indicating that crystals grows along the *c*-axis direction of apatite.[46] The carboxylic groups of gelatin at pH > 7 are mostly ionic, thus offer binding sites for Ca^{2+} and make the *c*-axis of HA crystal grow along the chain of gelatin.[39]

Proposed Self-Assembly Formation of Different Arranged Apatite Polycrystals in Hydrogels

Based on the obtained results, herein, the possible self-assemble mechanism of nanostructured carbonated apatite formation in hydrogels is shown in Scheme 1.

(1) In pure agar hydrogel, Ca^{2+} can't be chelated on agar surface due to lack of carboxyl groups for calcification. As verified from SEM and TEM observation, the crystals grown along the *a*, *b* and *c*-axis in the pores of hydrogel become flake-like.

(2) For gelatin solution, the –COOH groups existing on the surface of gelatin are in the form of –COO⁻ when the pH of solution is higher than isoelectric point (IEP) of gelatin.[47] These –COO⁻ as the active groups promote the binding of positive Ca^{2+} ions to gelatin surface, thus triggering the nucleation of apatite crystals. Under 37 °C, the forming needle-like apatite crystals grow along the gelatin chains and lead to rod-like crystals. However, subjected to a temperature of 65 °C for 3 days, gelatin undergoes thermal degradation and its single helix chain breaks into pieces.[44] The pieces chains with –COO⁻ could also chelate Ca^{2+}, and the smaller crystals with needle-like morphology grow on the surface of thermal degradation products. Those needle-like crystals could not self-assemble with continuous stirring.

(3) While in agar-gelatin hybrid hydrogel, the negatively charged functional groups on a portion of gelatin would react with the agar 3D network to form certain "bound side chains" by hydrogen bonding and electrostatic attraction, which is similar to the structure of proteoglycan complex.[48] Additionally, agar hydrogel can act as a delivery system for Ca^{2+} and PO_4^{3-} ions to control the reaction rate, and the interaction between gelatin fibers is enhanced by agar polysaccharide. The shift of FT-IR in Figure 3 indicates that gelatin act as a template during the formation of apatite. After that Ca^{2+} are attracted by –COO⁻ in gelatin through electrostatic interactions or by C=O and –OH in gelatin via polar interaction,[49] then *in situ* reacted with the subsequently diffused HPO_4^{2-} ions from supernatant to produce rod-like nanostructured apatite. At physiological temperature, these rode-like apatite crystals can self-assemble into nano-rod bundles through hydrogen bonding and electrostatic interaction between apatite and the gelatin macromolecule, such as electrostatic interaction between COO^- and Ca^{2+} and between $-NH_2$ and PO_4^{3-} of apatite.[50] So the bundle hierarchically crystals could be prepared in agar-gelatin hydrogel through the self-assembly of nanostructured apatite. The self-assembly procedure is similar to that of biomineralization in natrual bone,[3] as shown in Scheme 1. However, at 65 °C, the bonding between agar network and gelatin chains is weakened, and gelatin is broken down. Only needle-like crystals appear on the surface of the thermally degraded hydrogel. Overall, adding gelatin and changing temperature in the synthesis process could lead to the production of apatite with different Ca/P ratios, as well as distinct
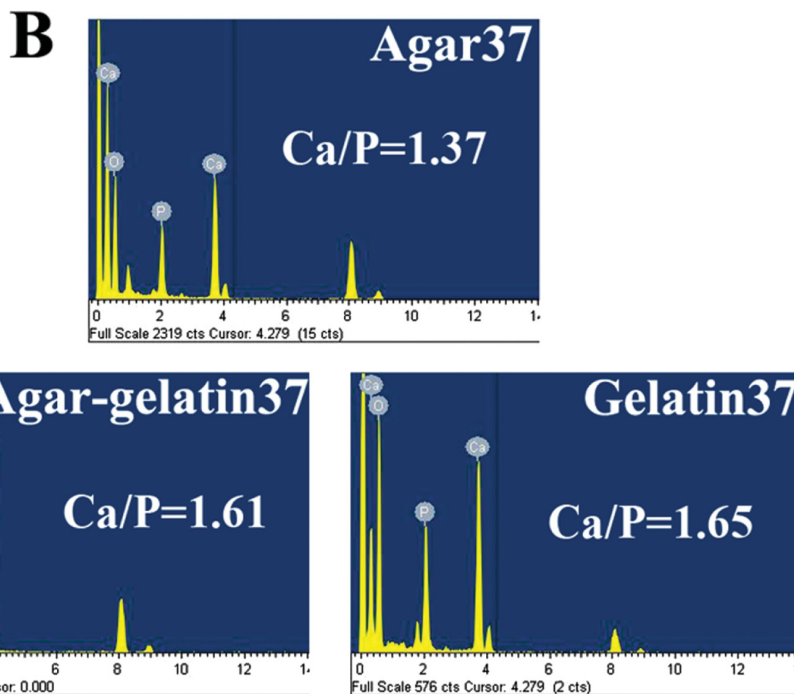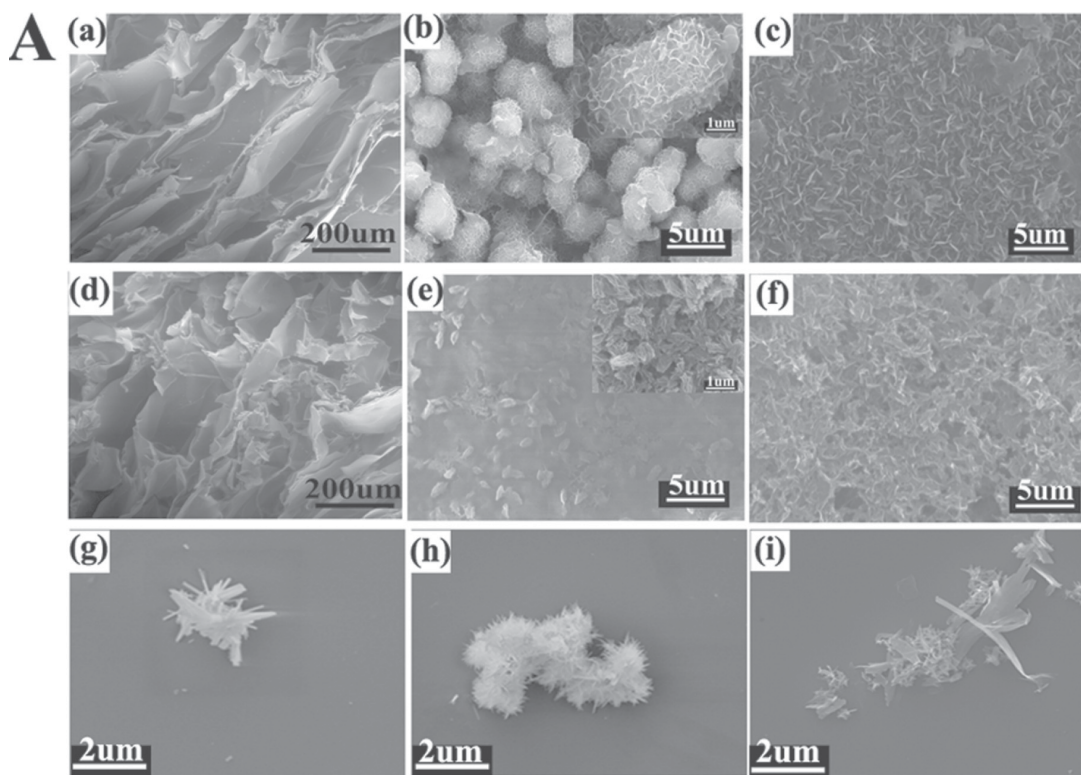
Figure 6. (A) SEM images of the agar-based hydrogels and as-prepared apatite under different conditions: (a) agar hydrogel; (b) Agar37; (c) Agar65; (d) agar-gelatin hybrid hydrogel; (e) Agar-gelatin37; (f) Agar-gelatin65; (g) Gelatin37; (h) Gelatin65 and (i) pure HA. The insets (b) and (e) show the high resolution SEM images of the corresponding apatite crystals. B is corresponding Energy Dispersive X-ray (EDX) spectroscopy.
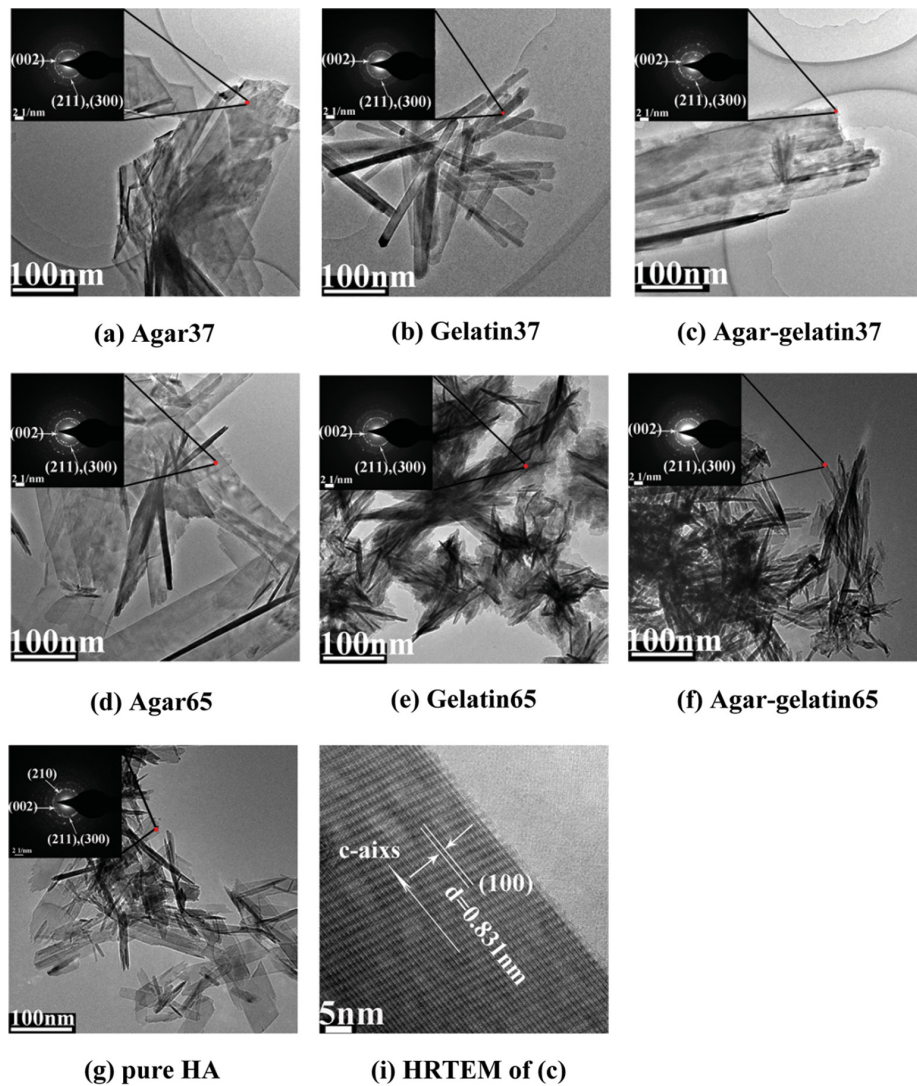
Figure 7. TEM and HRTEM micrographs of all as-prepared carbonated apatite in different conditions. The insets show the selected area electron diffraction (SAED) patterns of the corresponding apatite crystals.

morphologies. Nevertheless, the biological properties of apatites largely depend on its Ca/P ratio and morphology.

## The Biocompatibility of Carbonated Apatite

In Vitro Cytotoxicity Evaluation

The *in vitro* cytotoxicity of the as-prepared carbonated apatite was investigated using CCK-8 assay on MC3T3-E1 cell line. As shown in Figure 8, the cell proliferation increases with time goes on. At the first day, the viability of cells displays little statistical difference for each group. However, after incubating for 3 and 5 days, the cells show different proliferation rate. Especially, Agar37 and Agar65 groups show lower absorbance than control because the imperfect structure of OCP makes these crystals too chemically active.[51] Pure HA group featured irregular

morphology displays little bioactivity, good agreement with the results previously reported.[52] Nevertheless, higher cell viability has been obtained for the MC3T3 cells cultured with Agar-gelatin65 than others at 3 and 5 days. As mentioned above, the bone-like HA are thought to possess higher bioactivity, and it is also reported that calcium-deficient apatite is always of biological importance.[53] Meanwhile the residual gelatin on the obtained apatite could also promote the cell viability.

Alkaline Phosphatase Activity

Cell differentiation was investigated in terms of alkaline phosphatase activity of MC3T3 cells co-cultured with apatite for 7 days. Since alkaline phosphate at 7 days is expressed positively for the differentiation of
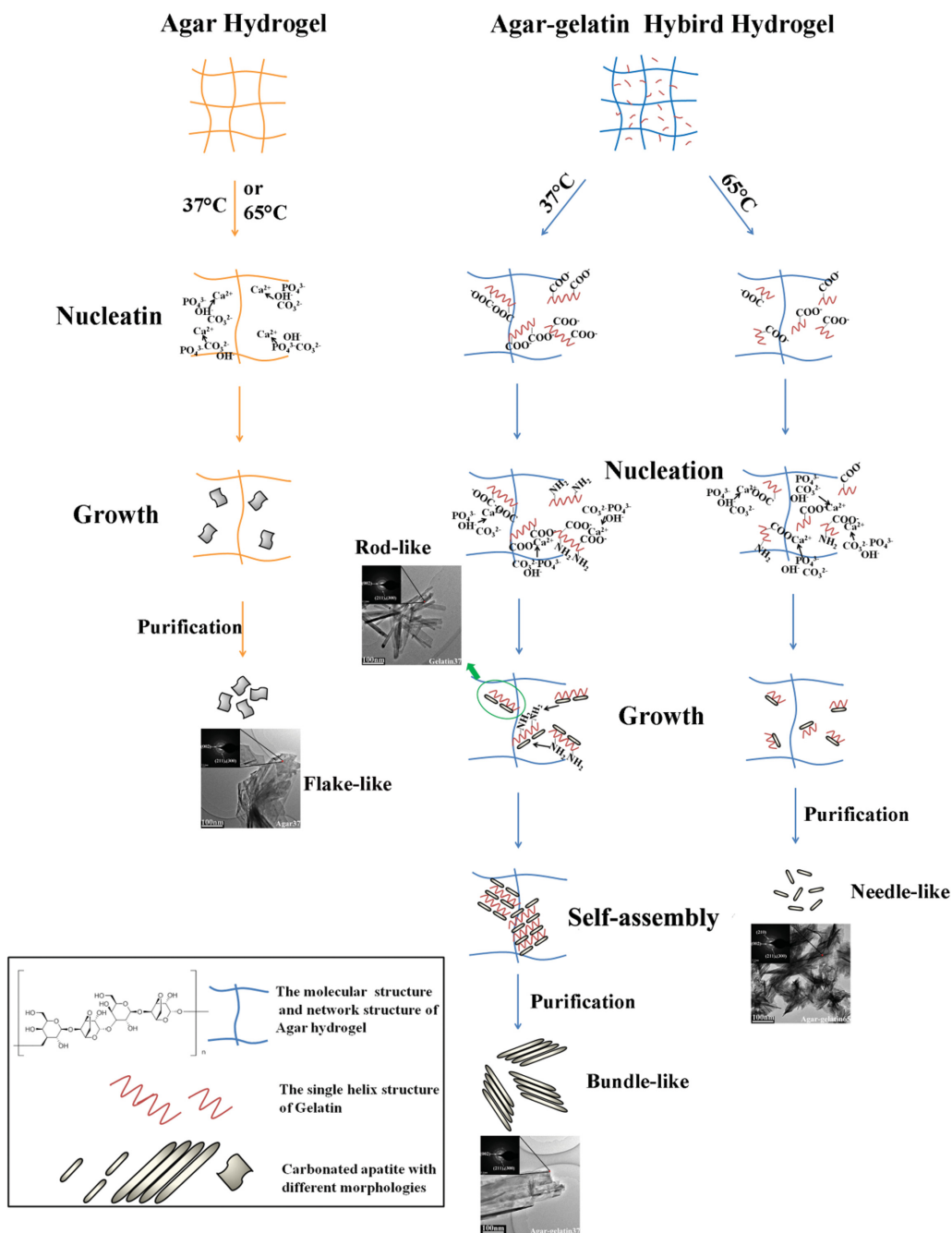
Scheme 1. Schematic drawing of the formation and self-assembling mechanism of the carbonated apatite in agar-based hydrogels.

MC3T3 cells, the assay is able to show early osteoblastic phenotypic expression.[54] It can be seen from Figure 9 that flake-like OCP crystals for Agar37 and Agar65 show lower ALP, because it is a possible precursor phase of apatite and performs worse osteogenic activity than carbonated apatite. Similarly, the best ALP expression is also detected in the Agar-gelatin37 group than other apatite groups,

indicating that the bone-like apatite could further enhance the mineralization and cell activation of the MC3T3 cells. The structure of agar and gelatin is similar to that of glycosaminoglycans (components of the extracellular matrix), and it has been reported that gelatin/HA composite can promote the expression of extracellular matrix proteins, and stimulate the differentiation of osteoprogenitor
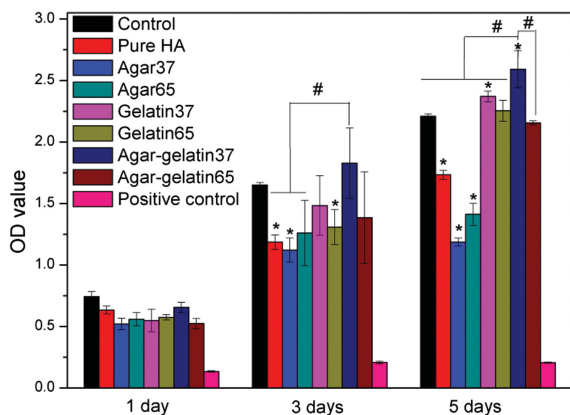
Figure 8. The cell proliferation rates of MC3T3-E1 cells cultured in media for 1 day, 3 days and 5 days, with different nanostructured apatite by CCK-8 analysis. ∗ represents $p < 0.05$ compared with the control group, and # represents $p < 0.05$ compared with Agar-gelatin65 group.
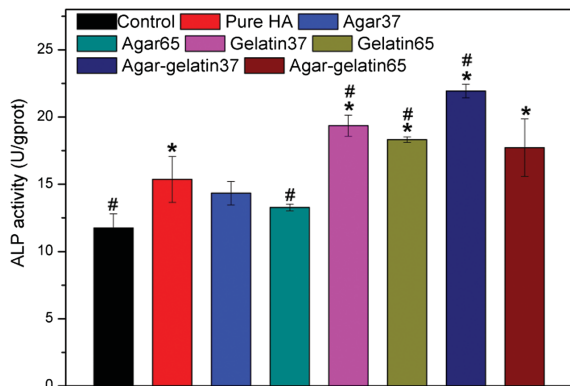

Figure 9. The ALP activity of MC3T3-E1 cells after cultivating with different nanostructured apatite for 7 days. ∗ represents $p < 0.05$ compared with the control, and # represents $p < 0.05$ compared with pure HA group.

cells, and ultimately facilitate bone formation.[55] As a consequence, the obtained carbonated apatite with bone-like morphology prepared by agar-gelatin co-hydrogel under physiological temperature presents excellent biocompatibility and outstanding *in vitro* bone bioactivity.

CONCLUSIONS

In summary, we report a facile biomimetic synthesis of carbonated apatite with bone-like morphology under physiological conditions using agar-gelatin hybrid hydrogel. The rod-like carbonated apatite assembled by ordered needle-shaped nano-crystals are formed, and aligned apaite assembly tightly bundled with rod-like nanostructured apatite in a hierarchical structure. The agar-gelaitn hybrid hydrogel not only could mediate the deposition of the mineral phase inside the 3D network, but also modulate the self-assembly of apatite through the surface functional groups (carboxyl

and amino moieties of gelatin, and Ca^{2+} and PO_4^{3-} groups of apatite). The *in vitro* biocompatibility tests reveal that the bone-like apatite prepared by agar-gelatin hydrogel is more favourable for the proliferation and differentiation of MC3T3-E1 compared to traditional method. Therefore, our *in vitro* study provides some insights into the possible roles of gelatin and polysaccharides involved in bone biomineralization, and the obtained apatite has great potential to be used in bone tissue engineering.

REFERENCES

1. A. Aravamudhan, D. M. Ramos, J. Nip, M. D. Harmon, R. James, M. Deng, C. T. Laurencin, X. Yu, and S. G. Kumbar, Cellulose and collagen derived micro-nano structured scaffolds for bone tissue engineering. *J. Biomed. Nanotechnol.* 9, 719 (**2013**).
2. A. J. Salgado, O. P. Coutinho, and R. L. Reis, Bone tissue engineering: State of the art and future trend. *Macromol. Biosci.* 4, 743 (**2004**).
3. J. Y. Rho, L. Kuhn-Spearing, and P. Zioupos, Mechanical properties and the hierarchical structure of bone. *Med. Eng. Phys.* 20, 92 (**1998**).
4. N. Saranya, S. Saravanan, A. Moorthi, B. Ramyakrishna, and N. Selvamurugan, Enhanced osteoblast adhesion on polymeric nanoscaffolds for bone tissue engineering. *J. Biomed. Nanotechnol.* 7, 238 (**2011**).
5. S. F. Ferrand, A. C. Mendoza-Palomares, F. Perrin-Schmitt, P. Netter, D. Mainard, P. Liverneaux, and N. Benkirane-Jessel, Bone formation induced by growth factors embedded into the nanostructured particles. *J. Biomed. Nanotechnol.* 7, 482 (**2011**).
6. P. Koley, M. G. B. Drew, and A. Pramanik, Salts responsive nanovesicles through π-stacking induced self-assembly of backbone modified tripeptides. *J. Nanosci. Nanotechnol.* 11, 6747 (**2011**).
7. J. Venkatesan and S. K. Kim, Stimulation of minerals by carbon nanotube grafted glucosamine in mouse mesenchymal stem cells for bone tissue engineering. *J. Biomed. Nanotechnol.* 8, 676 (**2012**).
8. N. Jamilpour, A. Fereidoon, and G. Rouhi, The effects of replacing collagen fibers with carbon nanotubes on the rate of bone remodeling process. *J. Biomed. Nanotechnol.* 7, 542 (**2011**).
9. K. C. Kavya, R. Dixit, R. Jayakumar, S. V. Nair, and K. P. Chennazhi, Synthesis and characterization of chitosan/chondroitin sulfate/nano-Sio2 composite scaffold for bone tissue engineering. *J. Biomed. Nanotechnol.* 8, 149 (**2012**).
10. M. Swetha, K. Sahithi, A. Moorthi, N. Saranya, S. Saravanan, K. Ramasamy, N. Srinivasan, and N. Selvamurugan, Synthesis, characterization, and antimicrobial activity of nano-hydroxyapatite-zinc for bone tissue engineering applications. *J. Biomed. Nanotechnol.* 12, 167 (**2012**).
11. G. E. Park and T. J. Webster, A review of nanotechnology for the development of better orthopedic implants. *J. Biomed. Nanotechnol.* 1, 18 (**2005**).
12. Y. Hao, H. Yan, X. Wang, B. Zhu, C. Ning, and S. Ge, Evaluation of osteoinduction and proliferation on nano-Sr-HAP: A novel orthopedic biomaterial for bone tissue regeneration. *J. Nanosci. Nanotechnol.* 12, 207 (**2012**).
13. G. D. Venkatasubbu, S. Ramasamy, V. Ramakrishnan, and J. Kumar, Hydroxyapatite-alginate nanocomposite as drug delivery matrix for sustained release of ciprofloxacin. *J. Biomed. Nanotechnol.* 7, 759 (**2011**).

14. P. Wang, C. Li, H. Gong, X. Jiang, H. Wang, and K. Li, Effects of synthesis conditions on the morphology of hydroxyapatite nanoparticles produced by wet chemical process. *Powder Technol.* 203, 315 (**2010**).

15. R. R. Rao, H. N. Roopa, and T. S. Kannan, Solid state synthesis and thermal stability of HAP and HAP-β-TCP composite ceramic powder. *J. Mater. Sci-Mater. M.* 8, 511 (**1997**).

16. T. Miyazaki, C. Ohtsuki, and M. Tanihara, Synthesis of bioactive organic-inorganic nanohybrid for bone repair through sol–gel processing. *J. Nanosci. Nanotechnol.* 3, 511 (**2003**).

17. Z. Xu, C. Liu, J. Wei, and J. Sun, Effects of four types of hydroxyapatite nanoparticles with different nanocystal morphologies and sizes on apoptosis in rat osteoblasts. *J. Appl. Toxicol.* 32, 429 (**2012**).

18. K.-I. Jeong, S.-G. Kim, J.-S. Oh, S.-Y. Lee, Y.-S. Cho, S.-S. Yang, S.-C. Park, J.-S. You, S.-C. Lim, M.-A. Jeong, J.-S. Kim, and S.-Y. Lee, Effect of platelet-rich plasma and platelet-rich fibrin on peri-implant bone defects in dogs. *J. Biomed. Nanotechnol.* 9, 535 (**2013**).

19. E. R. Wise, S. Maltsev, M. E. Davies, M. J. Duer, C. Jaeger, N. Loveridge, R. C. Murray, and D. G. Reid, The organic-mineral interface in bone is predominantly polysaccharide. *Chem. Mater.* 19, 5055 (**2007**).

20. V. Perla, M. Sato, and T. J. Webster, Increased skeletal muscle cell and osteoblast numbers on hydrothermally-treated nano-hydroxyapatite/collagen type I composites for entheses applications. *J. Biomed. Nanotechnol.* 1, 297 (**2005**).

21. Y. Wang, T. Azaïs, M. Robin, A. Vallée, C. Catania, P. Legriel, G. Pehau-Arnaudet, F. Babonneau, M.-M. Giraud-Guille, and N. Nassif, The predominant role of collagen in the nucleation, growth, structure and orientation of bone apatite. *Nat. Mater.* 11, 724 (**2012**).

22. X. Liu, L. A. Smith, J. Hu, and P. X. Ma, Biomimetic nanofibrous gelatin/apatite composite scaffolds for bone tissue engineering. *Biomaterials* 30, 2252 (**2009**).

23. M. Sadjadi, M. Meskinfam, B. Sadeghi, H. Jazdarreh, and K. Zare, *In situ* biomimetic synthesis and characterization of nano Hydroxyapatite in gelatin matrix. *J. Biomed. Nanotechnol.* 7, 450 (**2011**).

24. M. Gungormus, M. Branco, H. Fong, J. P. Schneider, C. Tamerler, and M. Sarikaya, Self assembled bi-functional peptide hydrogels with biomineralization-directing peptides. *Biomaterials* 31, 7266 (**2010**).

25. C. Zhong and C. C. Chu, Biomimetic mineralization of acid polysaccharide-based hydrogels: Towards porous 3-dimensional bone-like biocomposites. *J. Mater. Chem.* 22, 6080 (**2012**).

26. S. Gajjeraman, K. Narayanan, J. Hao, C. Qin, and A. George, Matrix macromolecules in hard tissues control the nucleation and hierarchical assembly of hydroxyapatite. *J. Biol. Chem.* 282, 1193 (**2007**).

27. L. Silverman and A. L. Boskey, Diffusion systems for evaluation of biomineralization. *Calcif . Tissue. Int.* 75, 494 (**2004**).

28. N. Bouropoulos and J. Moradian-Oldak, Induction of apatite by the cooperative Effect of amelogenin and the 32-kDa enamelin. *J. Dent. Res.* 83, 278 (**2004**).

29. C. Gobel, P. Simon, J. Buder, H. Tlatlik, and R. Kniep, Phase formation and morphology of calcium phosphate-gelatine-composites grown by double diffusion technique: the influence of fluoride. *J. Mater. Chem.* 14, 2225 (**2004**).

30. J. Sundaraseelan and T. Sastry, Fabrication of a Biomimetic compound containing nano hydroxyapatite-demineralised bone matrix. *J. Biomed. Nanotechnol.* 3, 401 (**2007**).

31. A. Ethirajan, U. Ziener, A. Chuvilin, U. Kaiser, H. Cölfen, and K. Landfester, Biomimetic hydroxyapatite crystallization in gelatin nanoparticles synthesized using a miniemulsion process. *Adv. Funct. Mater.* 18, 2221 (**2008**).

32. Y. Deng, Y. Sun, X. Chen, P. Zhu, and S. Wei, Biomimetic synthesis and biocompatibility evaluation of carbonated apatites template-mediated by heparin. *Mat. Sci. Eng. C* 33, 2905 (**2013**).

33. S. Zeng, S. Fu, G. Guo, H. Liang, Z. Qian, X. Tang, and F. Luo, Preparation and characterization of nano-hydroxyapatite/Poly(vinyl alcohol) composite membranes for guided bone regeneration. *J. Biomed. Nanotechnol.* 7, 549 (**2011**).

34. K. J. Payne and A. Veis, Fourier transform IR spectroscopy of collagen and gelatin solutions: Deconvolution of the amide I band for conformational studies. *Biopolymers* 27, 1749 (**1988**).

35. J. H. Lee, I. T. Kim, R. Tannenbaum, and M. L. Shofner, Synthesis of polymer-decorated hydroxyapatite nanoparticles with a dispersed copolymer template. *J. Mater. Chem.* 22, 11556 (**2012**).

36. R. Murugan and S. Ramakrishna, Production of ultra-fine bioresorbable carbonated hydroxyapatite. *Acta Biomater.* 2, 201 (**2006**).

37. L. Zhang, X. Feng, H. Liu, D. Qian, L. Zhang, X. Yu, and F. Cui, Hydroxyapatite/collagen composite materials formation in simulated body fluid environment. *Mater. Lett.* 58, 719 (**2004**).

38. M. Li, Y. Wang, Q. Liu, Q. Li, Y. Cheng, Y. Zheng, T. Xi, and S. Wei, *In situ* synthesis and biocompatibility of nano hydroxyapatite on pristine and chitosan functionalized graphene oxide. *J. Mater. Chem. B* 1, 475 (**2013**).

39. M. C. Chang, C.-C. Ko, and W. H. Douglas, Preparation of hydroxyapatite-gelatin nanocomposite. *Biomaterials* 24, 2853 (**2003**).

40. T. I. Ivanova, O. V. Frank-Kamenetskaya, A. B. Kol'tsov, and V. L. Ugolkov, Crystal structure of calcium-deficient carbonated hydroxyapatite, thermal decomposition. *J. Solid State Chem.* 160, 340 (**2001**).

41. M. G. Ma, Hierarchically nanostructured hydroxyapatite: Hydrothermal synthesis, morphology control, growth mechanism, and biological activity. *Int. J. Nanomed.* 7, 1781 (**2012**).

42. G. Falini, M. Gazzano, and A. Ripamonti, Control of the architectural assembly of octacalcium phosphate crystals in denatured collagenous matrices. *J. Mater. Chem.* 535, 2 (**2000**).

43. Y. Zhao, Y. Zhang, Y. Zhao, S. Hou, and P. K. Chu, Synthesis and cellular biocompatibility of two nanophase hydroxyapatite with different Ca/P ratio. *J. Nanosci. Nanotechnol.* 11, 11069 (**2011**).

44. I. Kilodziejska, E. Skierka, M. Sadowska, W. Kolodziejski, and C. Niecikowska, Effect of extracting time and temperature on yield of gelatin from different fish offal. *Food Chem.* 107, 700 (**2008**).

45. B. Viswanath and N. Ravishankar, Controlled synthesis of plate-shaped hydroxyapatite and implications for the morphology of the apatite phase in bone. *Biomaterials* 29, 4855 (**2008**).

46. H. Chen, B. H. Clarkson, K. Sun, and J. F. Mansfield, Self-assembly of synthetic hydroxyapatite nanorods into an enamel prism-like structure. *J. Colloid. Interf. Sci.* 288, 97 (**2005**).

47. C. He, F. Zhang, L. Cao, W. Feng, K. Qiu, Y. Zhang, H. Wang, X. Mo, and J. Wang, Rapid mineralization of porous gelatin scaffolds by electrodeposition for bone tissue engineering. *J. Mater. Chem.* 22, 2111 (**2012**).

48. W. D. Wagner, Proteoglycan structure and function as related to atherosclerosisa. *Ann. NY. Acad. Sci.* 454, 52 (**1985**).

49. M. C. Chang, T. Ikoma, M. Kikuchi, and J. Tanaka, Preparation of a porous hydroxyapatite/collagen nanocomposite using glutaraldehyde as a crosslinkage agent. *J. Mater. Sci. Lett.* 20, 1199 (**2001**).

50. Y. Ji Yin, F. Zhao, X. Feng Song, K. De Yao, W. W. Lu, and J. Chiyan Leong, Preparation and characterization of hydroxyapatite/chitosan-gelatin network composite. *J. Appl. Polym. Sci.* 77, 2929 (**2000**).

51. S. Kamakura, Y. Sasano, T. Shimizu, K. Hatori, O. Suzuki, M. Kagayama, and K. Motegi, Implanted octacalcium phosphate is more resorbable than β-tricalcium phosphate and hydroxyapatite. *J. Biomed. Mater. Res.* 59, 29 (**2002**).

52. Q. Li, M. Li, P. Zhu, and S. Wei, *In vitro* synthesis of bioactive hydroxyapatite using sodium hyaluronate as a template. *J. Mater. Chem.* 22, 20257 (**2012**).

53. J. A. S. Bett, L. G. Christner, and W. K. Hall, Hydrogen held by solids. XII. hydroxyapatite catalysts. *J. Am. Chem. Soc.* 89, 5535 (**1967**).

54. S. Hattar, A. Berdal, A. Asselin, S. Loty, D. Greenspan, and J. Sautier, Behaviour of moderately differentiated osteoblast-like cells cultured in contact with bioactive glasses. *Eur. Cell Mater.* 4, 61 (**2002**).

55. H. W. Kim, J. H. Song, and H. E. Kim, Nanofiber generation of gelatin-hydroxyapatite biomimetics for guided tissue regeneration. *Adv. Funct. Mater.* 15, 198 (**2005**).